Original Article | Neuroimaging and Head & Neck

eISSN 2005-8330
https://doi.org/10.3348/kjr.2019.0629
Korean J Radiol 2020;21(6):707-716

Korean Journal of Radiology
KJR

Prognostic Value of Dynamic Contrast-Enhanced MRI-Derived Pharmacokinetic Variables in Glioblastoma Patients: Analysis of Contrast-Enhancing Lesions and Non-Enhancing T2 High-Signal Intensity Lesions

Yeonah Kang, MD[1, 2], Eun Kyoung Hong, MD[3, 4], Jung Hyo Rhim, MD[2, 4], Roh-Eul Yoo, MD[3, 4], Koung Mi Kang, MD[3, 4], Tae Jin Yun, MD, PhD[3, 4], Ji-Hoon Kim, MD, PhD[3, 4], Chul-Ho Sohn, MD, PhD[3, 4], Sun-Won Park, MD, PhD[2, 4]*, Seung Hong Choi, MD, PhD[3, 4]*

[1]Department of Radiology, Haeundae Paik Hospital, Inje University College of Medicine, Busan, Korea; [2]Department of Radiology, Seoul Metropolitan Government-Seoul National University Boramae Medical Center, Seoul, Korea; [3]Department of Radiology, Seoul National University Hospital, Seoul, Korea; [4]Department of Radiology, Seoul National University College of Medicine, Seoul, Korea

Objective: To evaluate pharmacokinetic variables from contrast-enhancing lesions (CELs) and non-enhancing T2 high signal intensity lesions (NE-T2HSILs) on dynamic contrast-enhanced (DCE) magnetic resonance (MR) imaging for predicting progression-free survival (PFS) in glioblastoma (GBM) patients.

Materials and Methods: Sixty-four GBM patients who had undergone preoperative DCE MR imaging and received standard treatment were retrospectively included. We analyzed the pharmacokinetic variables of the volume transfer constant (Ktrans) and volume fraction of extravascular extracellular space within the CEL and NE-T2HSIL of the entire tumor. Univariate and multivariate Cox regression analyses were performed using preoperative clinical characteristics, pharmacokinetic variables of DCE MR imaging, and postoperative molecular biomarkers to predict PFS.

Results: The increased mean Ktrans of the CEL, increased 95th percentile Ktrans of the CELs, and absence of methylated O^6-methylguanine-DNA methyltransferase promoter were relevant adverse variables for PFS in the univariate analysis ($p = 0.041$, $p = 0.032$, and $p = 0.083$, respectively). The Kaplan-Meier survival curves demonstrated that PFS was significantly shorter in patients with a mean Ktrans of the CEL > 0.068 and 95th percentile Ktrans of the CEL > 0.223 (log-rank $p = 0.038$ and $p = 0.041$, respectively). However, only mean Ktrans of the CEL was significantly associated with PFS ($p = 0.024$; hazard ratio, 553.08; 95% confidence interval, 2.27–134756.74) in the multivariate Cox proportional hazard analysis. None of the pharmacokinetic variables from NE-T2HSILs were significantly related to PFS.

Conclusion: Among the pharmacokinetic variables extracted from CELs and NE-T2HSILs on preoperative DCE MR imaging, the mean Ktrans of CELs exhibits potential as a useful imaging predictor of PFS in GBM patients.

Keywords: *Dynamic contrast-enhanced MR imaging; Glioblastoma multiforme; Prognosis prediction; Parameter imaging; Preoperative analysis*

Received: August 21, 2019 **Revised:** December 31, 2019 **Accepted:** February 9, 2020

This study was supported by a grant from the Korea Healthcare technology R&D Projects, Ministry for Health, Welfare & Family Affairs (HI16C1111), by the Brain Research Program through the National Research Foundation of Korea (NRF) funded by the Ministry of Science, ICT & Future Planning (2016M3C7A1914002), by Basic Science Research Program through the National Research Foundation of Korea (NRF) funded by the Ministry of Science, ICT & Future Planning (2017R1A2B2006526), by Creative-Pioneering Researchers Program through Seoul National University (SNU), and by Project Code (IBS-R006-D1).

*These authors contributed equally to this work.

Corresponding author: Sun-Won Park, MD, PhD, Department of Radiology, Seoul Metropolitan Government-Seoul National University Boramae Medical Center, Seoul National University College of Medicine, 103 Daehak-ro, Jongno-gu, Seoul 03080, Korea.
• Tel: (822) 870-2544 • Fax: (822) 870-3539 • E-mail: swpark8802@gmail.com
Seung Hong Choi, MD, PhD, Department of Radiology, Seoul National University Hospital, Seoul National University College of Medicine, 103 Daehak-ro, Jongno-gu, Seoul 03080, Korea.
• Tel: (822) 3668-7832 • Fax: (822) 747-7418 • E-mail: verocay@snuh.org

INTRODUCTION

Glioblastoma (GBM) is an aggressive hypervascular malignant brain tumor that has infiltrative characteristics (1, 2). The median survival time is 14.6 months, despite the standard treatment of surgery followed by concomitant chemoradiotherapy (CCRT) with adjuvant temozolomide (3, 4). The surgical resection mainly targets contrast-enhancing tumors on contrast-enhanced T1-weighted images (T1WIs) (5), where the blood-brain barrier (BBB) is disrupted but which does not represent the solely viable tumor tissue.

As a previous study revealed, not only enhancing but also non-enhancing areas contain considerable amounts of infiltrative tumor with a high cellularity (1). Isolating infiltrative tumor cells is still challenging because these tumor cells are intermingled with reactive edema on T2-weighted image or T2 fluid-attenuated inverse recovery (FLAIR) images (2, 6, 7). This is reflected in the fact that we frequently encounter rapid local recurrence at the surgical margin, even after gross total resection. This might relate to the nature of the GBM being represented by immature and leaky neovascularization (8).

Analyzing the microvascular leakage of the tumor might be an important factor in predicting the tumor grade and prognosis (9). Thus far, many studies have reported using dynamic contrast-enhanced (DCE) magnetic resonance (MR) imaging, which is one of the methods that enable a quantitative analysis of angiogenesis and microvascular permeability (9-13). Gliomas with high permeability-related variables typically have a high histological grade (11). In a previous study of high-grade glioma patients, high permeability-related variables derived from DCE MR imaging served as a predictor of poor prognosis (13). This study focused on the contrast-enhancing tumors on contrast-enhanced T1WI; FLAIR was referenced only when there was no contrast-enhancing tumor on contrast-enhanced T1WI (13). In contrast, a recent study analyzed non-enhancing T2 high signal areas under an assumption that the pharmacokinetic variables from non-enhancing T2 high signal areas of GBM could identify infiltrative tumor cells outside the enhancing tumor resulting in permeability-related variables that could serve a candidate imaging biomarker (14).

However, to the best of our knowledge, there have been no studies comparing pharmacokinetic variables based on both contrast-enhancing lesions (CELs) and non-enhancing T2 high signal intensity lesions (NE-T2HSILs) of entire GBM areas using DCE MR imaging to predict disease progression. Hence, the purpose of our study was to evaluate the prognostic value of pharmacokinetic variables of DCE MR imaging from both CELs and NE-T2HSILs in the prediction of progression-free survival (PFS) in GBM patients.

MATERIALS AND METHODS

Study Population

This retrospective study was approved by the Institutional Review Board of our institution, Seoul National University College of Medicine and Seoul National University Hospital (IRB no. H-1712-118-908) and the requirement to obtain informed consent was waived.

From February 2012 to February 2017, 106 consecutive patients who were initially diagnosed with GBM and underwent preoperative DCE MR imaging at our institution were recruited. The inclusion criteria were as follows: the patient 1) had a histopathologic diagnosis of supratentorial GBM without other cell components based on the World Health Organization 2016 criteria, 2) underwent DCE MR imaging before surgery at our hospital and DCE raw data were available, and 3) underwent the standard treatment of gross-total resection, CCRT, and adjuvant temozolomide medication. Of these 106 patients, 42 were excluded for the following reasons: 1) lack of DCE data or data loading error (n = 11), 2) patients underwent surgical biopsy (n = 8), or 3) patients did not complete adjuvant temozolomide medication (n = 23). As a result, a total of 64 patients were included in this study. O^6-methylguanine-DNA methyltransferase (MGMT) promoter methylation status and isocitrate dehydrogenase (IDH) mutation were also investigated. Clinical variables, such as age, sex, and Karnofsky performance score (KPS), were recorded.

All patients visited the outpatient clinic after completion of the standard treatment comprising CCRT with temozolomide followed by adjuvant temozolomide medication. Additionally, patients underwent regular follow-up MR imaging after CCRT until there was evidence of clinical deterioration as defined by tumor progression or death. The median follow-up period was 14.4 months (range, 2.6–56.8 months). The flow diagram of patient selection and classification is shown in Figure 1.

PFS

On the basis of the clinical features and radiologic data,

https://doi.org/10.3348/kjr.2019.0629

Korean Journal of Radiology
KJR

the patients were categorized into either the disease progression or stable disease according to the Response Assessment in Neuro-Oncology criteria in each visit (6). We only recorded the first progression. PFS was defined as the calculated from the date of the diagnosis until progression, verified clinically and on MR imaging, or until the last follow-up date, if no progression or death occurred.

MR Image Acquisition

MR imaging of all patients was performed by using one of two 3T MR imaging units (Verio or Skyra; Siemens Healthineers, Erlangen, Germany). We adopted a fixed T1 method (T1 of 1000 ms) in calculating the baseline T1 to obtain consistent data from DCE MR imaging although the T1 measurement method provides physiologic tissue properties (15-17). MR scan variables are summarized in Supplementary Table 1.

Image Processing and Analysis

The post processing of DCE MR imaging was performed by a dedicated commercial software package (NordicICE, version 2.3.12; NordicNeuroLab, Bergen, Norway). Based on the two-compartment pharmacokinetic model suggested by Tofts and Kermode (18), the volume transfer constant (Ktrans) and volume fraction of extravascular extracellular space (Ve) were calculated. Deconvolution with the arterial input function (AIF) was performed in the pharmacokinetic model. For each tumor, the AIF was determined in intracranial tumor-supplying arteries near the tumor. The co-registration between the structural images (transverse FLAIR images and contrast-enhanced T1WI) and parametric maps from DCE MR imaging was automatically performed by an algorithm that found the most appropriate transformation, based on the geometric information stored in the respective data sets (19, 20).

Two neuroradiologists (with 5 and 16 years of experience in neuroradiology, respectively) chose an appropriate AIF curve to show the ideal relationship between the AIF curve and concentration-time curve (17). Subsequently, with the consent of the two neuroradiologists, a region of interest (ROI) was manually drawn along the margin of the CEL on the parametric map co-registered with each axial structural contrast-enhanced T1WI. In the same manner, the ROI for NE-T2HSIL was drawn on the parametric map co-registered with each axial structural FLAIR image; therefore, they could define the margin of the NE-T2HSIL with confidence. The ROI of both CELs and NE-T2HSILs were defined excluding cystic or necrotic regions and macrovessels. On a pixel-by-pixel basis, pharmacokinetic variables were calculated from the ROI on every transverse image. The overall values for each tumor were obtained by summing the values from every axial plane. Finally, the parametric values from the total CEL and NE-T2HSIL were acquired and recorded for each tumor. A simplified diagram of the image processing methods is depicted in Figure 2.

To evaluate the reproducibility of pharmacokinetic variables, we randomly selected 20 patients. Each

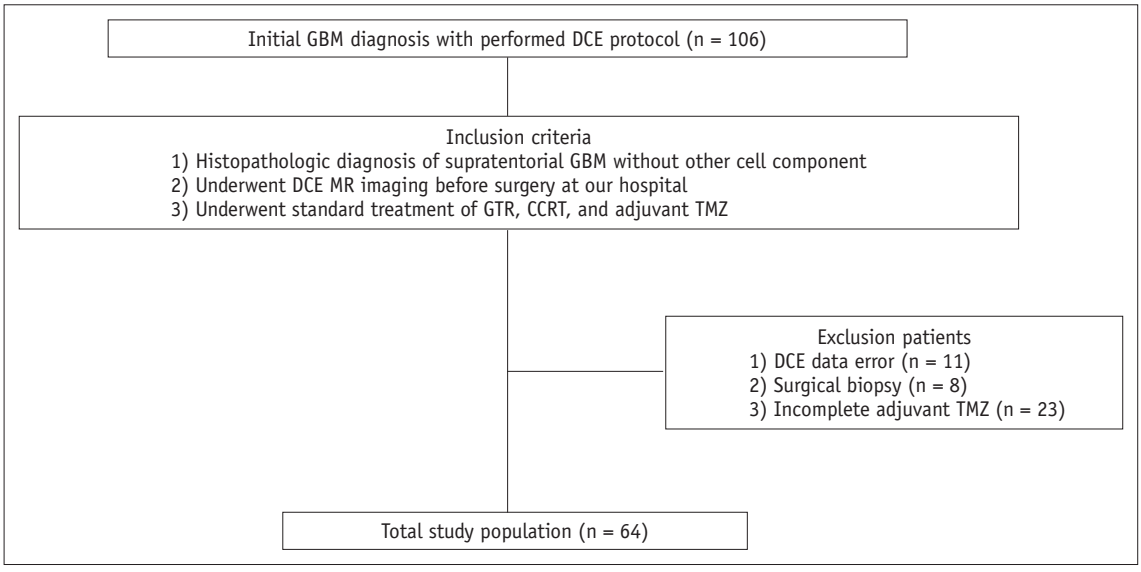

Fig. 1. Flowchart shows selection of study population. CCRT = concomitant chemoradiotherapy, DCE = dynamic contrast-enhanced, GBM = glioblastoma, GTR = gross-total resection of contrast-enhancing lesions, MR = magnetic resonance, TMZ = temozolomide

https://doi.org/10.3348/kjr.2019.0629

procedure, including AIF selection and ROI plotting in every axial plane of the NE-T2HSIL on FLAIR images and CEL on contrast-enhanced T1WI, was performed by another radiologist with 4 year experience in neuroradiology. The interobserver reproducibility was calculated from the data acquired from two independent readers (one from initial analysis and the other from an additional reader).

Statistical Analysis

All statistical analyses were performed using MedCalc statistical software, version 11.1.1.0 (MedCalc, Mariakerke, Belgium), SPSS Statistics software, version 20.0 for Windows (IBM Corp., Armonk, NY, USA), and R for Windows version 3.0.2. The mean value and 95th percentile of each variable were calculated and are denoted in the text by the indices $\_mean$ and $\_95th$, respectively.

Univariate Cox regression analysis was performed to identify predictors of PFS among the following variables: age, sex, KPS, genetic information including MGMT and IDH status, tumor volume, and pharmacokinetic variables on DCE MR imaging; all variables with $p < 0.1$ were considered to be relevant and included in the multivariate Cox proportional hazard analysis. Prognostic performance was assessed by calculating the Harrell concordance index (c-index). Patients were classified into either the disease progression or non-progression groups based on their status at 14.6 months from the date of the diagnosis, described as the median survival after standard treatment in a previous study (4). To obtain optimum cutoff values for the pharmacokinetic variables, the significant pharmacokinetic variables on univariate Cox regression were analyzed using the area under the receiver operating characteristic curve (AUC) (19). Leave-one-out cross-validation was also performed to validate the diagnostic performance. The distribution of PFS was estimated using Kaplan-Meier survival curves and compared using a log-rank test. The interobserver

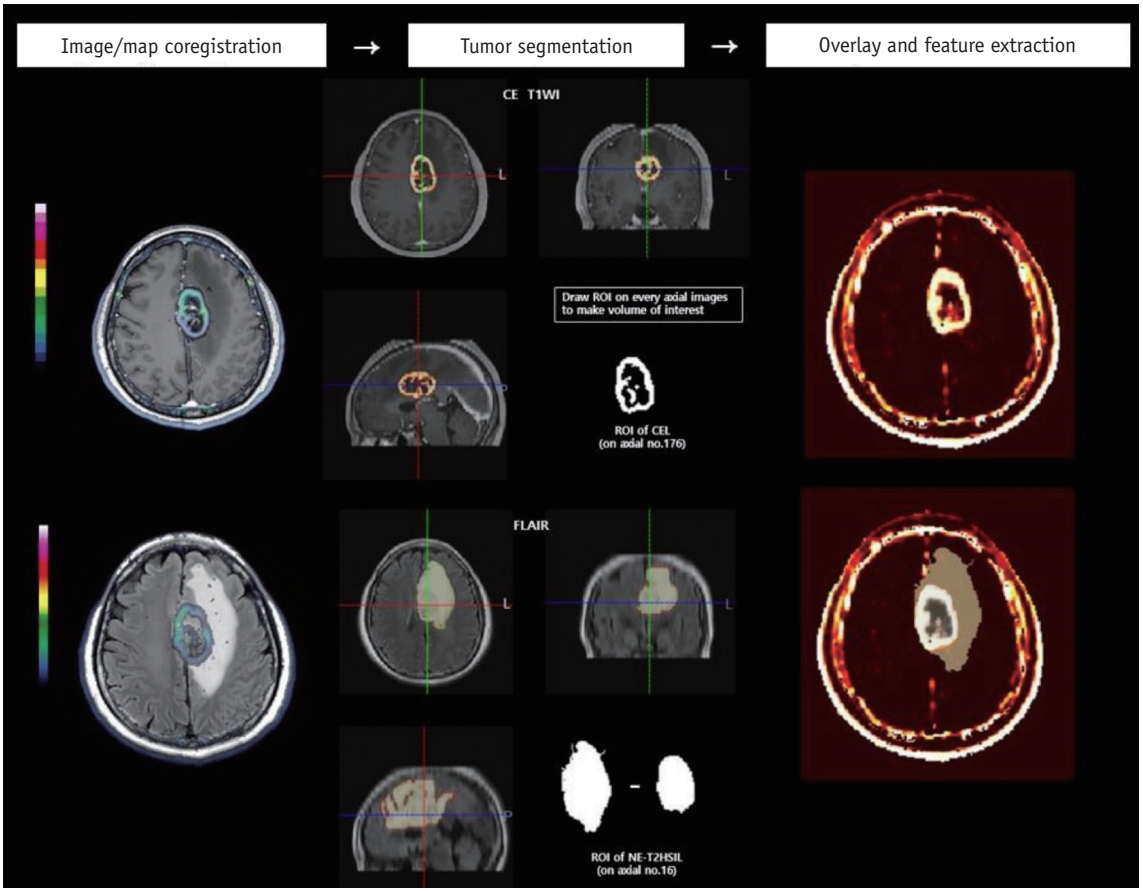

Fig. 2. Simplified diagram of image processing. Structural images (CE T1WI and FLAIR) are co-registered with parametric maps (Ktrans and Ve). ROIs were drawn in each axial slice of structural images to obtain VOIs for CELs on CE T1WI and for NE-T2HSILs on FLAIR, respectively. VOIs are overlaid on parametric maps. Quantitative features of tumor were then extracted and analyzed. CEL = contrast-enhancing lesion, CE T1WI = contrast-enhanced T1-weighted image, FLAIR = fluid-attenuated inverse recovery, Ktrans = volume transfer constant, NE-T2HSIL = non-enhancing T2 high signal intensity lesion, ROI = region of interest, Ve = volume fraction of extravascular extracellular space, VOI = volume of interest

https://doi.org/10.3348/kjr.2019.0629

Korean Journal of Radiology
KJR

reproducibility was assessed by using the intraclass correlation coefficient (ICC). We adapted the following guidelines for the ICC: 0.00–0.20 was considered to indicate slight agreement, 0.21–0.40 fair agreement, 0.41–0.60 moderate agreement, 0.61–0.80 substantial agreement, and 0.81–1.00 almost perfect agreement (20).

RESULTS

Clinical Characteristics

Baseline clinical characteristics of the patients, including age, sex, Karnofsky performance scale, MGMT methylation status, IDH mutation status, volume of the CEL, and volume of the NE-T2HSIL are summarized in Table 1.

Survival Analysis

In the univariate Cox proportional hazard analysis, the absence of methylated MGMT promoter, increased $Ktrans_{\_mean}$ of the CEL, and increased $Ktrans_{\_95th}$ of the CEL were relevant adverse variables for PFS ($p = 0.041$, $p = 0.032$, and $p = 0.083$, respectively). In the multivariate Cox proportional hazard analysis, only $Ktrans_{\_mean}$ of the CEL was significantly associated with PFS ($p = 0.024$; hazard ratio, 553.08; 95% confidence interval [CI], 2.27–134756.74; c-index, 0.676) (Table 2, Fig. 3).

Table 1. Patient Clinical Characteristics

Clinical Characteristic	Total Patients (n = 64)
Age (years)	55.6 (± 13.9)
Sex	
Male	39 (60.9)
Female	25 (39.1)
Karnofsky performance scale	
< 70	8 (12.5)
≥ 70	56 (87.5)
Genetic information	
Methylated MGMT promoter	
Negative	23 (35.9)
Positive	41 (64.1)
IDH mutation	
Mutant	6 (9.4)
Wild type	58 (90.6)
Tumor volume (mL)	
CEL	111.9 (± 583.3)
NE-T2HSIL	66.0 (± 42.2)

Age and tumor volume are expressed as mean (± standard deviation); other variables are expressed as numbers (%). CEL = contrast-enhancing lesion, IDH = isocitrate dehydrogenase, MGMT = O^6-methylguanine-DNA methyltransferase, NE-T2HSIL = non-enhancing T2 high signal intensity lesion

Diagnostic Performance and Predicting Disease Progression Using DCE Pharmacokinetic Variables

The optimal cutoff values and AUCs for the quantitative variables of $Ktrans_{\_mean}$ and $Ktrans_{\_95th}$ of the CEL were as follows: $Ktrans_{\_mean}$ of the CEL, 0.068 and 0.666 (AUC range, 0.520–0.792; sensitivity of 88.2%, specificity of 44.1%); $Ktrans_{\_95th}$ of the CEL, 0.223 and 0.659 (AUC range, 0.511–0.757; sensitivity of 94.1%, specificity of 38.2%); $p = 0.034$ and $p = 0.040$, respectively. The leave-one-out cross-validation for Ktrans_mean of the CEL demonstrated a sensitivity of 100% and specificity of 37.5%. The Kaplan-Meier survival curves demonstrated that PFS was significantly shorter in patients with $Ktrans_{\_mean}$ of the CEL > 0.068, and $Ktrans_{\_95th}$ of the CEL > 0.223 (log-rank $p = 0.038$ and $p = 0.041$, respectively). Unmethylated MGMT was also a significant predictor of poor PFS ($p = 0.025$); moreover, combining $Ktrans_{\_mean}$ of the CEL and MGMT status further stratified prognosis in patients with GBMs ($p = 0.014$) (Fig. 4).

Interobserver Reproducibility of DCE Pharmacokinetic Variables

The ICC for CEL was excellent; the ICC for $Ktrans_{\_mean}$, $Ve_{\_mean}$, $Ktrans_{\_95th}$, and $Ve_{\_95th}$ were 0.995 (95% CI, 0.988–0.998), 0.978 (95% CI, 0.944–0.991), 0.999 (95% CI, 0.998–1.000), and 0.942 (95% CI, 0.852–0.977), respectively, revealing almost perfect agreement. Meanwhile, interobserver agreement of the NE-T2HSIL varied from slight to moderate agreement ($Ktrans_{\_mean}$, $Ve_{\_mean}$, $Ktrans_{\_95th}$, and $Ve_{\_95th}$ were 0.087 [95% CI, -1.306–0.639], 0.215 [95% CI, -0.983–0.689], 0.467 [95% CI, -0.346–0.789], and 0.406 [95% CI, -0.500–0.765]).

DISCUSSION

In this retrospective study, we evaluated DCE-MR imaging-derived permeability variables that were extracted from both CELs and NE-T2HSILs to predict the prognosis of GBM. Among various pharmacokinetic DCE variables and clinical variables, we discovered that $Ktrans_{\_mean}$ of the CEL was the only independent predictor of progression in the multivariate analysis.

Previous studies have recognized that contrast enhancement on preoperative conventional MR imaging is a significant factor associated with survival in patients with GBM (21, 22). However, a mouse glioma study revealed that BBB disruption was present in brain tumors before evidence

https://doi.org/10.3348/kjr.2019.0629

Table 2. Univariate and Multivariate Survival Analysis

Variables	Univariate Analysis		Multivariate Analysis	
	Hazard Ratio (95% CI)	*P*	Hazard Ratio (95% CI)	*P*
Age	1.01 (0.98–1.04)	0.253		
Sex		0.153		
Male	1 (reference)			
Female	0.60 (0.30–1.20)			
Karnofsky performance		0.426		
< 70	1 (reference)			
≥ 70	0.66 (0.25–1.72)			
Genetic information				
Methylated MGMT promoter		0.041	1.96 (0.92–4.14)	0.070
Negative	2.07 (1.05–4.10)			
Positive	1 (reference)			
IDH mutation		0.448		
Mutant	0.64 (0.19–2.13)			
Wild type	1 (reference)			
Tumor volume				
CEL	0.99 (0.99–1.00)	0.433		
NE-T2HSIL	1.00 (0.99–1.01)	0.177		
DCE parameters				
CEL				
$Ktrans_{\_mean}$	553.08 (2.26–134799.10)	0.032	553.08 (2.27–134756.74)	0.024
$Ktrans_{\_95th}$	4.85 (0.91–25.70)	0.083	1.85 (0.03–111.03)	0.733
$Ve_{\_mean}$	1.01 (0.99–1.02)	0.294		
$Ve_{\_95th}$	1.00 (0.99–1.01)	0.324		
NE-T2HSIL				
$Ktrans_{\_mean}$	4.28×10^{-15} (1.79×10^{-43}–102.19×10^{12})	0.291		
$Ktrans_{\_95th}$	0.66 (0.00–1544.07)	0.935		
$Ve_{\_mean}$	0.87 (0.64–1.17)	0.338		
$Ve_{\_95th}$	0.99 (0.95–1.03)	0.711		

CI = confidence interval, DCE = dynamic contrast-enhanced, Ktrans = volume transfer constant, Ve = volume of extravascular extracellular space

of angiogenesis was observed (23). In other words, contrast enhancement of tumors on conventional MR imaging does not require neovascularization and that disruption of the BBB can be caused by other mechanisms (23). In addition, those previous studies used subjective criteria, which might lead to decreased reproducibility (21, 22). In this study, we performed quantitative analysis of neoangiogenesis and vascular permeability using DCE MR imaging.

There have been some reports based on DCE MR imaging regarding the prediction of survival and prognosis in GBM patients (13, 14, 24). Choi et al. (24) suggested that higher Ktrans and Ve values of enhancing tumors are associated with worse prognosis in GBM patients. In high grade glioma patients, Ulyte et al. (13) reported that Ve was a significant predictor of PFS and overall survival. They mainly focused on enhancing tumors and referred to the FLAIR image only when there was no contrast enhancement on the contrast-enhanced T1WI. On the other hand, Kim et al. (14) analyzed non-enhancing T2 high-signal areas in GBM and determined that the 99th percentile value of Ktrans was an independent imaging biomarker of early disease progression following standard treatment. Their study only included DCE MR variables of NE-T2HSIL to derive their results; hence, the result did not include the intrinsic properties of the initial enhancing tumors. Considering the result that CELs had higher Ktrans and Ve values than those of NE-T2HSIL in our study, we assume that the inherent aggressive nature of tumors is more apparent in enhancing tumors than in NE-T2HSIL, which is an interminglement of infiltrative non-enhancing tumor and reactive edema. Therefore, we speculate that the Ktrans derived from CELs better reflects the characteristics of the tumor and is more relevant to

https://doi.org/10.3348/kjr.2019.0629

Korean Journal of Radiology
KJR

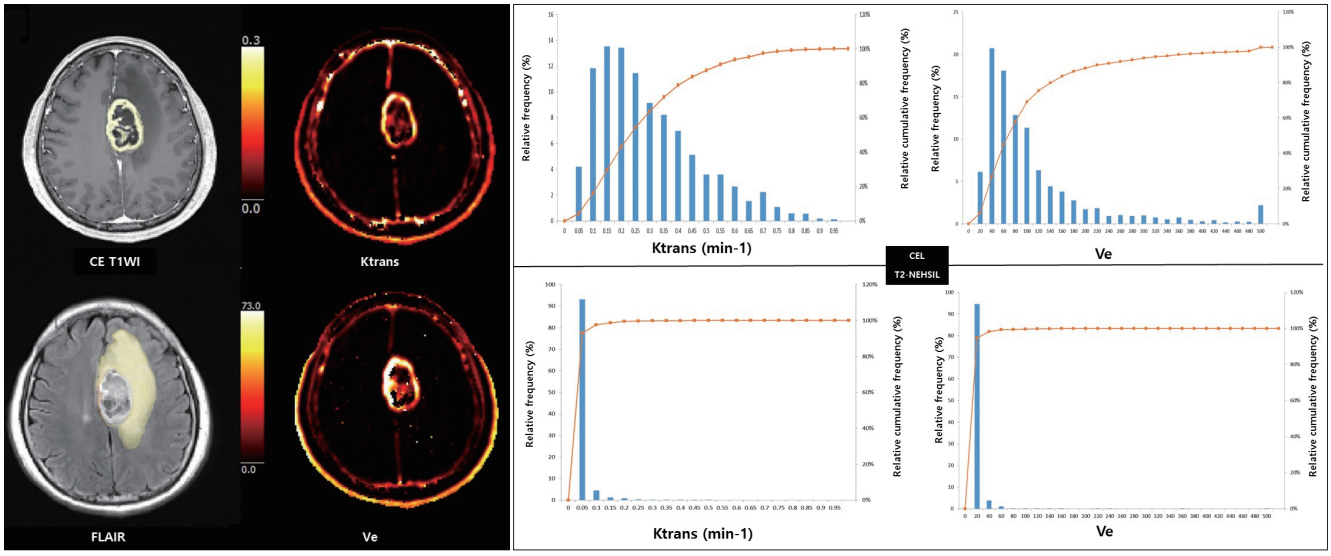

A

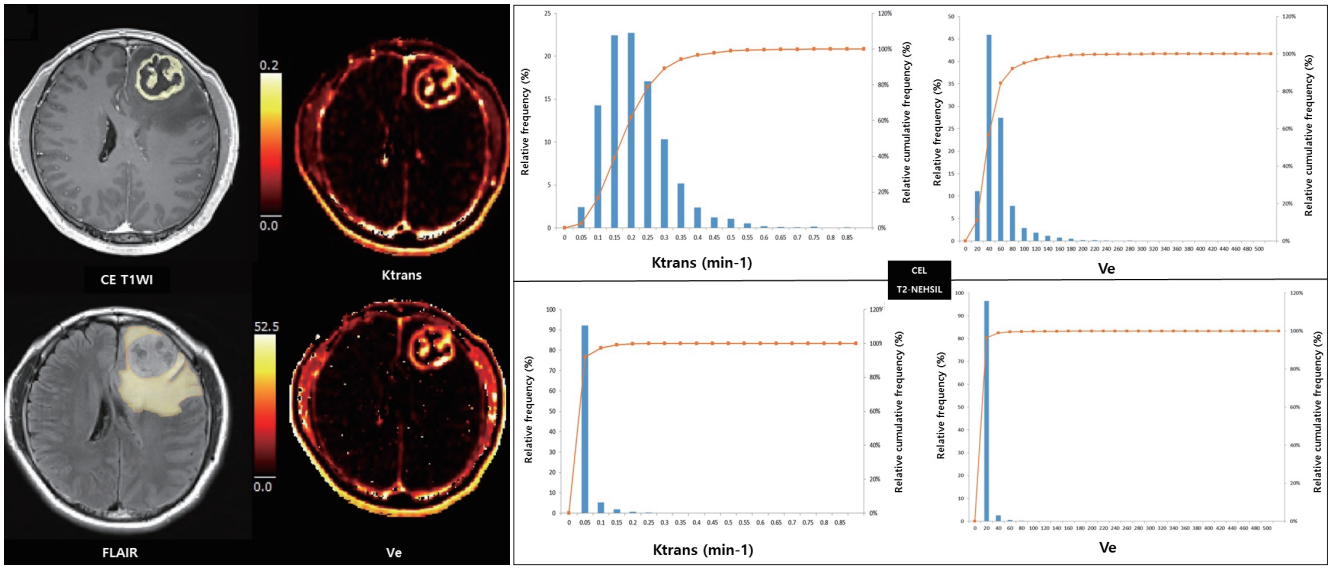

B

Fig. 3. Representative dynamic contrast-enhanced MR imaging-derived pharmacokinetic variable maps in patients whose GBM had progressed (A) and had not progressed (B) after standard treatment. A. 53-year-old GBM patient who had early disease progression after standard treatment (PFS = 9 months). Preoperative transverse CE T1WI and FLAIR images show ROI of CEL and surrounding NE-T2HSIL, respectively. Preoperative pharmacokinetic DCE parametric maps of Ktrans and Ve in CEL show higher values as compared with those of surrounding NE-T2HSIL. **B.** 43-year-old GBM patient who did not progress after standard treatment (PFS = 55 months). On histograms for pharmacokinetic variables, lines represent relative cumulative frequencies of Ktrans and Ve. Histograms of CEL of patient **(B)** show rightward shift as compared with corresponding histograms in **(A)**, suggesting that frequencies of low values were higher in patients who had not progressed than patients with early disease progression. PFS = progression-free survival

the patient's prognosis after standard treatment. To our knowledge, evaluation of the prognostic value of both CEL and NE-T2HSIL based on preoperative DCE MR imaging in GBM patients after standard treatment has not been established in previous research. We analyzed permeability-related variables in both enhancing and non-enhancing tumors to evaluate which of these variables were more relevant to disease progression. We found that the $Ktrans_{mean}$ of CELs had a significant impact on survival in contrast to the permeability-related variables from NE-T2HSILs.

In this study, we analyzed markers of permeability, Ktrans and Ve, among the variables derived from DCE MR imaging (25). Ktrans is the volume transfer constant between the plasma and extravascular extracellular space, which reflects vascular permeability. As the higher Ktrans values predict a higher tumor grade, aggressive glioma

 https://doi.org/10.3348/kjr.2019.0629

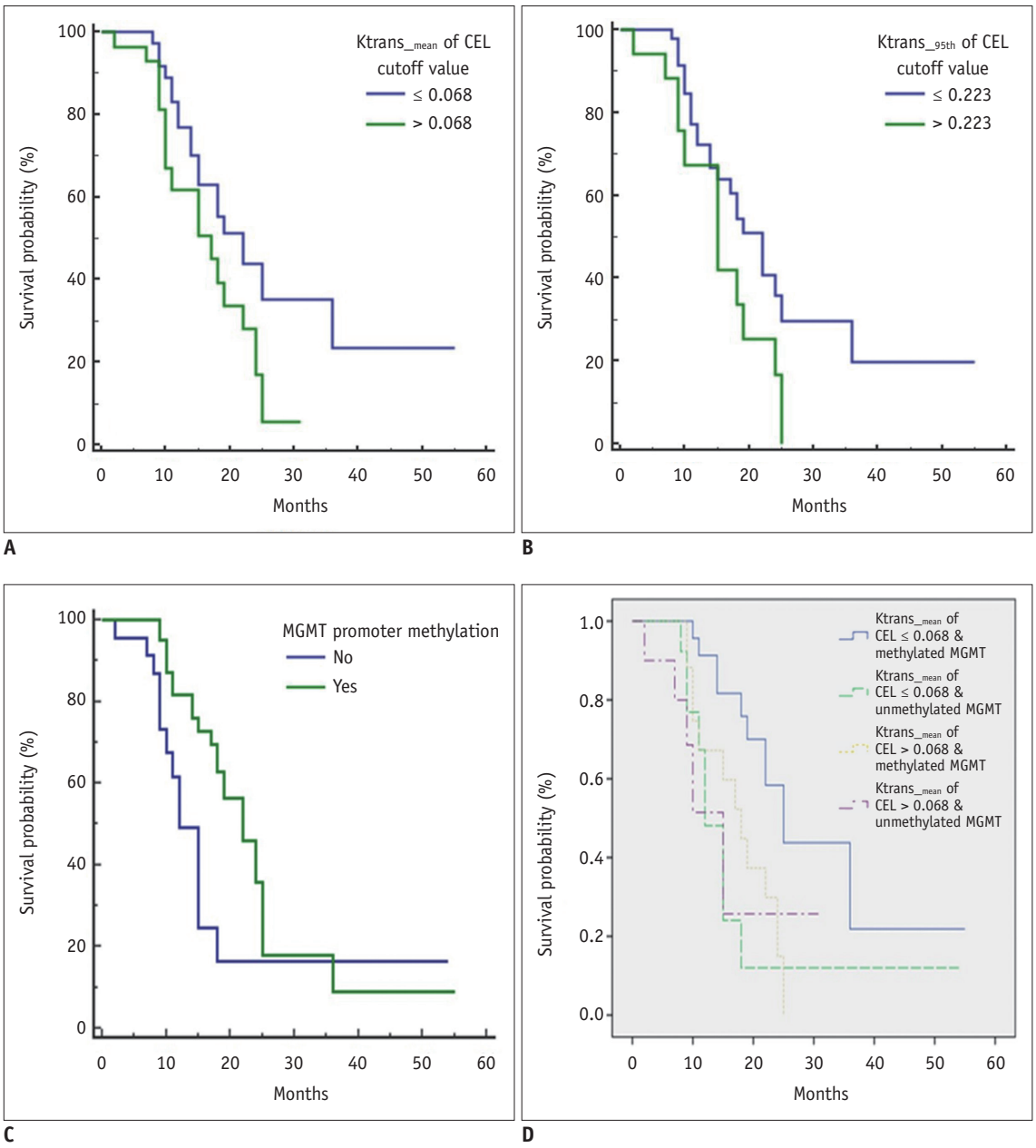

Fig. 4. Kaplan-Meier curve for PFS.
A. Ktrans$_{mean}$ of CELs (p = 0.038). **B.** Ktrans$_{95th}$ of CELs (p = 0.041). **C.** MGMT promoter methylation (p = 0.025). **D.** Combination of Ktrans$_{mean}$ of CEL and MGMT promoter methylation (p = 0.014). MGMT = O^6-methylguanine-DNA methyltransferase

may require more neoangiogenesis, resulting in a higher proportion of immature leaky vessels (13, 14, 26, 27). We speculate that not only do the DCE permeability variables of CELs play an important role in predicting survival, but also immature and leaky neovascularization progresses more actively in the CELs than in the NE-T2HSILs of GBM. Our result might be correlated with previous MR imaging-immunohistochemical pathologic finding correlation studies, which have demonstrated that compared with those from non-enhancing regions, pretreatment tissue biopsy samples from contrast-enhancing regions had increased microvascular expression, simple and complex hyperplastic microvasculature, cellular density, and architectural disruption (2, 28).

Our study had several limitations. First, this study has the inevitable weaknesses associated with any retrospective study. We included patients who completed standard treatment; consequently, patients with tumors of an aggressive nature who could not survive six cycles of adjuvant chemotherapy might not have been selected.

https://doi.org/10.3348/kjr.2019.0629

Korean Journal of Radiology
KJR

However, our hospital routinely performs DCE MR imaging for patients with GBM who are treated with a standard regimen. Hence, our cohort study might serve as a potential representative sample. Second, interobserver agreement on the DCE pharmacokinetic variables of the NE-T2HSIL lesions varied from slight to moderate agreement. This might be the cause of discrepancy between our findings and a previous study that analyzed non-enhancing T2 high-signal areas in GBM (14). We retrospectively analyzed the inter-rater agreement for volume measurements derived from the NE-T2HSIL segmentations using the ICC that resulted in moderate agreement (0.593 [95% CI, 0.228–0.812]). This result might explain that different subjective views when determining the boundaries of infiltrative T2 high signal intensity affects the reproducibility of pharmacokinetic variables derived from NE-T2HSILs. By contrast, the interobserver agreement for CELs showed almost perfect agreement between the DCE pharmacokinetic variables. Finally, further study is recommended for the standardization of the DCE MR imaging protocol and data analysis.

In conclusion, the pharmacokinetic variables that were derived through preoperative DCE MR imaging could serve as prognostic imaging biomarkers. Among the pharmacokinetic variables extracted from CELs and NE-T2HSILs, the most significant variable was $Ktrans_{\_mean}$ of CELs, which can be a useful clinical imaging biomarker, especially in predicting PFS of GBM patients.

Supplementary Materials

The Data Supplement is available with this article at https://doi.org/10.3348/kjr.2019.0629.

Conflicts of Interest

The authors have no potential conflicts of interest to disclose.

ORCID iDs

Sun-Won Park
https://orcid.org/0000-0002-5063-2685
Seung Hong Choi
https://orcid.org/0000-0002-0412-2270
Yeonah Kang
https://orcid.org/0000-0002-5078-3213
Eun Kyoung Hong
https://orcid.org/0000-0002-5440-0451
Jung Hyo Rhim
https://orcid.org/0000-0001-5822-9770
Roh-Eul Yoo
https://orcid.org/0000-0002-5625-5921
Koung Mi Kang
https://orcid.org/0000-0001-9643-2008
Tae Jin Yun
https://orcid.org/0000-0001-8441-4574
Ji-Hoon Kim
https://orcid.org/0000-0002-6349-6950
Chul-Ho Sohn
https://orcid.org/0000-0003-0039-5746

REFERENCES

1. Eidel O, Burth S, Neumann JO, Kieslich PJ, Sahm F, Jungk C, et al. Tumor infiltration in enhancing and non-enhancing parts of glioblastoma: a correlation with histopathology. *PLoS One* 2017;12:e0169292
2. Barajas RF Jr, Phillips JJ, Parvataneni R, Molinaro A, Essock-Burns E, Bourne G, et al. Regional variation in histopathologic features of tumor specimens from treatment-naive glioblastoma correlates with anatomic and physiologic MR Imaging. *Neuro Oncol* 2012;14:942-954
3. Oh J, Henry RG, Pirzkall A, Lu Y, Li X, Catalaa I, et al. Survival analysis in patients with glioblastoma multiforme: predictive value of choline-to-N-acetylaspartate index, apparent diffusion coefficient, and relative cerebral blood volume. *J Magn Reson Imaging* 2004;19:546-554
4. Stupp R, Mason WP, van den Bent MJ, Weller M, Fisher B, Taphoorn MJ, et al. Radiotherapy plus concomitant and adjuvant temozolomide for glioblastoma. *N Engl J Med* 2005;352:987-996
5. Albert FK, Forsting M, Sartor K, Adams HP, Kunze S. Early postoperative magnetic resonance imaging after resection of malignant glioma: objective evaluation of residual tumor and its influence on regrowth and prognosis. *Neurosurgery* 1994;34:45-60; discussion 60-61
6. Wen PY, Macdonald DR, Reardon DA, Cloughesy TF, Sorensen AG, Galanis E, et al. Updated response assessment criteria for high-grade gliomas: response assessment in neuro-oncology working group. *J Clin Oncol* 2010;28:1963-1972
7. Norden AD, Drappatz J, Muzikansky A, David K, Gerard M, McNamara MB, et al. An exploratory survival analysis of anti-angiogenic therapy for recurrent malignant glioma. *J Neurooncol* 2009;92:149-155
8. Hardee ME, Zagzag D. Mechanisms of glioma-associated neovascularization. *Am J Pathol* 2012;181:1126-1141
9. Jain R. Measurements of tumor vascular leakiness using DCE in brain tumors: clinical applications. *NMR Biomed* 2013;26:1042-1049
10. Jia Z, Geng D, Xie T, Zhang J, Liu Y. Quantitative analysis

of neovascular permeability in glioma by dynamic contrast-enhanced MR imaging. *J Clin Neurosci* 2012;19:820-823
11. Jung SC, Yeom JA, Kim JH, Ryoo I, Kim SC, Shin H, et al. Glioma: application of histogram analysis of pharmacokinetic parameters from T1-weighted dynamic contrast-enhanced MR imaging to tumor grading. *AJNR Am J Neuroradiol* 2014;35:1103-1110
12. Cao Y, Nagesh V, Hamstra D, Tsien CI, Ross BD, Chenevert TL, et al. The extent and severity of vascular leakage as evidence of tumor aggressiveness in high-grade gliomas. *Cancer Res* 2006;66:8912-8917
13. Ulyte A, Katsaros VK, Liouta E, Stranjalis G, Boskos C, Papanikolaou N, et al. Prognostic value of preoperative dynamic contrast-enhanced MRI perfusion parameters for high-grade glioma patients. *Neuroradiology* 2016;58:1197-1208
14. Kim R, Choi SH, Yun TJ, Lee ST, Park CK, Kim TM, et al. Prognosis prediction of non-enhancing T2 high signal intensity lesions in glioblastoma patients after standard treatment: application of dynamic contrast-enhanced MR imaging. *Eur Radiol* 2017;27:1176-1185
15. Nam JG, Kang KM, Choi SH, Lim WH, Yoo RE, Kim JH, et al. Comparison between the prebolus T1 measurement and the fixed T1 value in dynamic contrast-enhanced MR imaging for the differentiation of true progression from pseudoprogression in glioblastoma treated with concurrent radiation therapy and temozolomide chemotherapy. *AJNR Am J Neuroradiol* 2017;38:2243-2250
16. Tietze A, Mouridsen K, Mikkelsen IK. The impact of reliable prebolus T_1 measurements or a fixed T_1 value in the assessment of glioma patients with dynamic contrast enhancing MRI. *Neuroradiology* 2015;57:561-572
17. Haacke EM, Filleti CL, Gattu R, Ciulla C, Al-Bashir A, Suryanarayanan K, et al. New algorithm for quantifying vascular changes in dynamic contrast-enhanced MRI independent of absolute T_1 values. *Magn Reson Med* 2007;58:463-472
18. Tofts PS, Kermode AG. Measurement of the blood-brain barrier permeability and leakage space using dynamic MR imaging. 1. Fundamental concepts. *Magn Reson Med* 1991;17:357-367
19. Sundar H, Shen D, Biros G, Xu C, Davatzikos C. Robust computation of mutual information using spatially adaptive meshes. *Med Image Comput Comput Assist Interv* 2007;10(Pt 1):950-958
20. Pluim JP, Maintz JB, Viergever MA. Mutual-information-based registration of medical images: a survey. *IEEE Trans Med Imaging* 2003;22:986-1004
21. Lacroix M, Abi-Said D, Fourney DR, Gokaslan ZL, Shi W, DeMonte F, et al. A multivariate analysis of 416 patients with glioblastoma multiforme: prognosis, extent of resection, and survival. *J Neurosurg* 2001;95:190-198
22. Hammoud MA, Sawaya R, Shi W, Thall PF, Leeds NE. Prognostic significance of preoperative MRI scans in glioblastoma multiforme. *J Neurooncol* 1996;27:65-73
23. Cha S, Johnson G, Wadghiri YZ, Jin O, Babb J, Zagzag D, et al. Dynamic, contrast-enhanced perfusion MRI in mouse gliomas: correlation with histopathology. *Magn Reson Med* 2003;49:848-855
24. Choi YS, Kim DW, Lee SK, Chang JH, Kang SG, Kim EH, et al. The added prognostic value of preoperative dynamic contrast-enhanced MRI histogram analysis in patients with glioblastoma: analysis of overall and progression-free survival. *AJNR Am J Neuroradiol* 2015;36:2235-2241
25. Aref M, Chaudhari AR, Bailey KL, Aref S, Wiener EC. Comparison of tumor histology to dynamic contrast enhanced magnetic resonance imaging-based physiological estimates. *Magn Reson Imaging* 2008;26:1279-1293
26. Bisdas S, Smrdel U, Bajrovic FF, Surlan-Popovic K. Assessment of progression-free-survival in glioblastomas by intratreatment dynamic contrast-enhanced MRI. *Clin Neuroradiol* 2016;26:39-45
27. Nguyen TB, Cron GO, Perdrizet K, Bezzina K, Torres CH, Chakraborty S, et al. Comparison of the diagnostic accuracy of DSC- and dynamic contrast-enhanced MRI in the preoperative grading of astrocytomas. *AJNR Am J Neuroradiol* 2015;36:2017-2022
28. Barajas RF Jr, Hodgson JG, Chang JS, Vandenberg SR, Yeh RF, Parsa AT, et al. Glioblastoma multiforme regional genetic and cellular expression patterns: influence on anatomic and physiologic MR imaging. *Radiology* 2010;254:564-576

https://doi.org/10.3348/kjr.2019.0629